

SCRNet: Spatial-Channel Regulation Network for Medical Ultrasound Image Segmentation

Weixin Xu¹, Ziliang Wang^{*2}
¹Beihang University, ²Peking University
^{*}Corresponding Author

Abstract—Medical ultrasound image segmentation presents a formidable challenge in the realm of computer vision. Traditional approaches rely on Convolutional Neural Networks (CNNs) and Transformer-based methods to address the intricacies of medical image segmentation. Nevertheless, inherent limitations persist, as CNN-based methods tend to disregard long-range dependencies, while Transformer-based methods may overlook local contextual information. To address these deficiencies, we propose a novel Feature Aggregation Module (FAM) designed to process two input features from the preceding layer. These features are seamlessly directed into two branches of the Convolution and Cross-Attention Parallel Module (CCAPM) to endow them with different roles in each of the two branches to help establish a strong connection between the two input features. This strategy enables our module to focus concurrently on both long-range dependencies and local contextual information by judiciously merging convolution operations with cross-attention mechanisms. Moreover, by integrating FAM within our proposed Spatial-Channel Regulation Module (SCRM), the ability to discern salient regions and informative features warranting increased attention is enhanced. Furthermore, by incorporating the SCRM into the encoder block of the UNet architecture, we introduce a novel framework dubbed Spatial-Channel Regulation Network (SCRNet). The results of our extensive experiments demonstrate the superiority of SCRNet, which consistently achieves state-of-the-art (SOTA) performance compared to existing methods.

Index Terms—Medical Ultrasound Image, Segmentation, Breast, Thyroid

I. INTRODUCTION

Medical ultrasound image segmentation is critical in pre-treatment diagnoses, treatment planning, and post-treatment assessments of various diseases. In recent years, benefiting from the ability to obtain representative features, convolutional neural networks (CNNs) have been widely applied in medical image segmentation tasks. Specifically, UNet [1], which employs an encoder-decoder structure with skip connections to achieve remarkable performance in medical image segmentation, was proposed. Benefiting from the sophisticated encoder-decoder architecture and the exquisitely designed skip connections, several variants of UNet, such as ResUNet [2], UNet++ [3], and UNet3+ [4], have been proposed and have performed well in different medical image segmentation challenges. However, even though these CNN-based methods have exhibited satisfactory performance, some limitations still exist, such as the loss of the long-range dependencies among pixels. These limitations come from CNN itself. Therefore, avoiding them through architectural design seems infeasible.

For this reason, some methods [5]–[7] have tried to incorporate attention modules [8] in their architectures to enhance the feature map for better pixel-level classification of medical images with impressive performance improvement. However, these methods still cannot avoid the problem of capturing insufficient long-range dependencies.

With the transformer proposed, the problem of missing long-range dependencies can be effectively solved. Transformer [9] was first proposed to solve the problem of machine translation in the field of natural language processing (NLP). Based on this, vision transformers (ViTs) [10] have been proposed for computer vision tasks. In summary, ViTs perform well on computer vision tasks, such as image classification, and semantic segmentation, because they leverage self-attention/cross-attention to learn correlations among all the input tokens and therefore can enable the models to capture long-range dependencies. Moreover, ViTs divide an image into non-overlapping patches that are fed into the transformer module with positional embeddings. Based on ViTs, several methods [11], [12] have been proposed for medical image segmentation by importing transformer blocks as the middle layers. Notably, this combination has indeed achieved satisfactory performance with the transformer architectures. However, the self-attention/cross-attention used in transformers limits their ability to learn local (contextual) relations among pixels, which are as important as global information when addressing medical image segmentation tasks.

In this paper, to solve the above issues, we propose a novel Feature Aggregation Module (FAM) that combines global and local features that establish connections with each other to better refine information from the extracted features. Moreover, to better extract informative feature maps and avoid disturbance from non-informative redundancy features, we propose a spatial-channel regulation module (SCRM) to progressively suppress features in irrelevant background regions. Our main contributions are summarized as follows:

- We propose the novel **Feature Aggregation Module (FAM)**, which can establish connections between different features from previous layers and simultaneously learn local relations and long-range dependencies by aggregating feature maps from convolution operations and cross-attention. Therefore, this module can help integrate features from different operations to better refine information.

- Based on the FAM, we introduce **Spatial-Channel Regulation Module (SCRM)**, which can help determine whether features are informative or non-informative. Specifically, the SCRM consists of two components: **Spatial Gate (SG)**, which is utilized to determine where to focus, and **Channel Refinement (CR)**, which determines what to focus on.
- By incorporating the SCRM into the encoder blocks of the UNet, we introduce a new framework dubbed **Spatial-Channel Regulation Network (SCRNet)**. We evaluate our proposed SCRNet on the BUSI, BUSIS, and TN3K datasets, which are widely used public benchmarks for medical ultrasound image segmentation tasks. Extensive experiments are conducted to evaluate the performance of the proposed methods for medical ultrasound image segmentation, which shows state-of-the-art (SOTA) performance.

II. RELATED WORK

A. CNN-based image segmentation

Long et al. [1] first proposed a fully convolutional network (FCN) to complete the semantic segmentation task by classifying images at the pixel level. Although the results obtained are still not refined enough, FCN proposes a new paradigm for solving semantic segmentation problems. Noh et al. [13] proposed a deep deconvolution structure and applied it to the semantic segmentation task for the first time, which effectively solves the problem of the limitations of FCN networks that cannot effectively handle small objects. Based on FCN and Deconvolution, Segnet [14] was proposed, which first introduced skip connections in deep learning as a solution to the information loss observed in typical downsampling layers of encoder-decoder networks. This helps to reduce information loss through aggressive pooling and downsampling, helping to recover finer object localization. PSPNet [15] proposes a pyramid pooling module, Spatial Pyramid Pooling (SPP), which is mainly designed around multi-scale information and global context modeling. At the same time, it uses the idea of GoogleNet [16] to introduce auxiliary loss to help the network converge better. RefineNet [17] aims to model the information interaction between multiple levels of features, and at the same time combines the residual idea to help the network's gradient return, making the overall training of the model easier to converge; in addition, the Chained Residual Pooling module is applied to capture more context information. DFN [18] mainly addresses the two major challenges faced by semantic segmentation tasks: intra-class inconsistency and inter-class indistinction and proposes a corresponding feature discriminative network, Discriminative Feature Network, which includes Smooth Network and Border Network, specifically, Smooth Network is used to deal with intra-class consistency issues, and Border Network is used to deal with unclear boundaries. PSANet [19] proposes a point-wise Spatial Gate mechanism for scene parsing tasks, which alleviates local neighborhood constraints by adaptively learning an attention mask that associates each location on the feature map with other locations.

B. Transformer-based image segmentation

Dosovitskiy et al. [10] first introduce Vision Transformers (ViTs), which achieve outstanding performance due to capturing long-range dependencies among the pixels. Inspired by this, many transformer-based semantic segmentation methods are proposed. SETR [20] is one of the first representative works to introduce ViT into the semantic segmentation framework. The UN-EPT [21] network uniformly considers contextual information and boundary artifacts to segment objects. First, a sparse sampling strategy is applied to incorporate a Transformer-based attention mechanism for efficient context modeling. Finally, a separate spatial branch is introduced to capture image details for boundary refinement, and the whole model can be trained in an end-to-end manner. From a multi-scale perspective, PVT [22] introduces the pyramid structure into ViT to better complete dense prediction tasks. The overall structure of SegFormer [23] continues to use hierarchical feature representation to capture multi-scale features, and at the same time removes the position embedding in the original ViT structure, avoiding the problem of model performance degradation caused by the different sizes of the test image and the training image. Finally, in the decoder part, an MLP structure is applied to aggregate feature maps of different scales from the encoder output to simultaneously fuse local attention and global attention. Segmenter [24] is a network structure built on a pure Transformer block to model global context information and use a point-wise linear decoder or a mask Transformer to obtain class labels.

C. Medical image segmentation

Medical image segmentation is a challenging task that needs to classify the dense pixels of organs or lesions in a given medical image. In recent years, many meaningful models are proposed to tackle medical image segmentation tasks. The most notable one, UNet [1], proposed to use the annotated samples more efficiently by capturing information of context. Following UNet, lots of variants are proposed to solve different problems. Specifically, ResUNet [2] and DenseUNet [25] are respectively inspired by residual connections and dense connections, replacing each sub-module of UNet with residual connections and dense connections. Based on the ResUNet, ResUNet++ [26] introduces squeeze and excitation block, ASPP, and attention block into ResUNet. UNet++ [3] strengthens information interaction by integrating features at different levels; and designs a flexible network structure with deep supervision, allowing a deep network with a huge amount of parameters to greatly reduce the number of parameters within an acceptable accuracy range. Attention UNet [5] proposes a model based on gated attention, which can suppress the background area, emphasize the foreground area, and automatically learn how to distinguish the shape and size of the target.

CNN-based methods have shown impressive performance on medical image segmentation tasks, but they still have limitations in obtaining long-range dependencies. Some methods proposed to incorporate transformer blocks to solve this

limitation. Li et al. [27] introduce TFCNs by combining transformer and fully convolutional DenseNet to propagate semantic features and filter out non-semantic features. CAST-former [28] is a hybrid network structure composed of CNN + Transformer, which captures rich global spatial information and local multi-scale context information by integrating multi-scale pyramid structures. In addition, the strategy of further applying generative adversarial training is used to improve segmentation performance, enabling Transformer-based discriminators to capture low-level anatomical features and high-level semantics. Cao et al. [29] proposed Swin-UNet, which is a pure transformer architecture based on Swin transformer [30]. Swin-UNet uses transformers in both the encoder and decoder, which does not lead to performance improvement.

Many methods try to incorporate transformer blocks with convolution blocks and achieve satisfactory performance. However, just combining them directly by plain workflow without any feature interaction will bring information loss to some extent. In contrast, in our FAM, we processed the features by increasing interaction with each other and carefully designed the combination manner of convolution and cross-attention mechanism to maintain long-range dependencies and local context information better together.

III. METHOD

A. Spatial-Channel Regulation Module

To enhance the quality of our feature maps, we have integrated Spatial-Channel Regulation Modules (SCRM) into our methodology. These modules encompass two pivotal constituents: Spatial Gate (SG) and Channel Refinement (CR).

Spatial Gate (SG): Spatial Gate determines where to focus in a feature map and then enhances those features. As shown in Figure 1, Spatial Gate consists of the following steps: First, a softmax operation followed by the scaling factors in group-normalization (GN) [31] layers are utilized to assess the informative content of different feature maps W_{info} , which calculated as eq.(1). Subsequently, we normalize the weight values of feature maps, W_{info} , to the range (0, 1) using the sigmoid function and apply a threshold of 0.5 to gate these values. This process is mathematically defined as Equation (2). During this step, we obtain informative weights, denoted as W_1 , by setting weights in W above the threshold to 1. We also obtain non-informative weights, denoted as W_2 , by setting weights in W below the threshold to 0. Following this, we perform element-wise multiplication of the two sets of weighted outputs, W_1 and W_2 , with the input feature X . Consequently, this yields two sets of weighted features: the informative ones, X_{w1} , and the less informative ones, X_{w2} .

$$W_{info} = GN(X) \times Softmax(GN(X)) \quad (1)$$

$$W = Threshold(Sigmoid(W_{info})) \quad (2)$$

Additionally, X_{w1} is bifurcated into two constituents performed by averaging based on the number of channels, results are denoted as X_{w1}^1 and X_{w1}^2 , while X_{w2} is similarly separated

into X_{w2}^1 and X_{w2}^2 . Afterward, we meticulously rearranged and consolidated these four components to derive the ultimate outputs by the Reconstruct operation shown in Figure 1. Following these procedures, we ascertain the informativeness of specific features while discerning non-informative ones. The procedural steps are formulated as eq. (3), where \oplus represents element-wise summation, and \cup represents concatenation.

$$\begin{cases} X_{w1} = X_{w1}^1 \cup X_{w1}^2 \\ X_{w2} = X_{w2}^1 \cup X_{w2}^2 \\ X_{out} = Concat(X_{w1}^1 \oplus X_{w2}^2, X_{w1}^2 \oplus X_{w2}^1) \end{cases} \quad (3)$$

Channel Refinement (CR): Channel Refinement identifies which feature maps to focus on and then refine them. As shown in Figure 1, the Channel Refinement consists of the following steps: First, for giving input features from the previous Spatial Gate layer, X_{out} , we split the N channels of X_{out} into two parts with $N \times W$ channels and $N \times (1 - W)$ channels, where $0 \leq W \leq 1$. Next, 1×1 convolutions are utilized on those two feature maps so that the channels can be squeezed, therefore we get two feature maps as X_{C1} and X_{C2} . Then, for the X_{C1} , we adopt efficient convolution operations, group-wise convolution (GWC) and point-wise convolution (PWC), to extract high-level representations. Afterward, the two outputs are summed together to get the final output features as X_H . The calculating process is shown in eq.(4). For the X_{C2} , we only use the PWC operation to extract low-level representations and then concat the output features with the X_{C2} to get the final output features as X_L , as shown in eq.(5). Following the acquisition of X_H and X_L , those two feature maps are fed into our proposed **Feature Aggregation Module (as elaborated in section III-B)** to get the final output so that we can identify the informative feature maps and better refine them by interacting with each other.

$$X_H = GWC(X_{C1}) + PWC(X_{C1}) \quad (4)$$

$$X_L = Concat(X_{C2}, PWC(X_{C2})) \quad (5)$$

B. Feature Aggregation Module

The architecture of our proposed Feature Aggregation Module (FAM) is depicted in Figure 2. Our design is underpinned by the following fundamental observations: 1). Traditional methods of feature aggregation often resort to rudimentary operations such as concatenation or summation. These methods are inherently limited in their ability to effectively synthesize the extracted features, as they tend to retain extraneous or potentially irrelevant information from prior operations. 2). While convolution operations are widely employed for feature extraction, they are not without their limitations. Firstly, convolutions primarily focus on local representations, as their receptive field size is contingent upon the kernel size. Furthermore, conventional convolutions lack memory functionality, making it challenging to establish robust interconnections

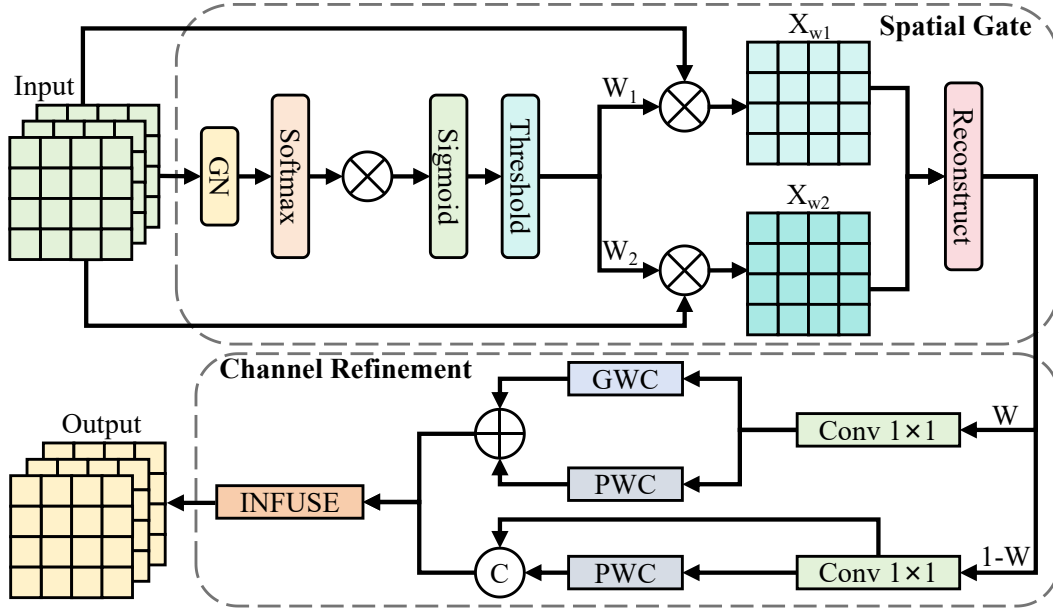


Fig. 1. The framework of our proposed Spatial-Channel Regulation Module. The GN represents the group-normalization, the GWC represents the group-wise convolution, and the PWC represents the point-wise convolution.

among diverse features solely through convolutional operations. Drawing inspiration from these observations, we introduce the novel Feature Aggregation Module. This module's core purpose is to establish robust connections among distinct features, facilitating the seamless integration of information and eliminating interference from extraneous data.

The workflow of our proposed FAM is as follows. Two inputs from preceding layers, denoted as X_H and X_L , are fed into two **Convolution & Cross Attention Parallel Modules (CCAPMs)**, details of which are presented in Section III-B1. This strategic allocation optimizes the feature extraction process by enabling them to play distinct yet complementary roles and engage in purposeful interactions. Moreover, participating in different roles to interact with each other can provide more effective information and establish a closer connection. Following this interaction, the two resultant outputs from the CCAPMs are harmoniously fused to yield the ultimate results. This fusion operation is instrumental in the assimilation of essential information while concurrently eliminating irrelevant and extraneous features. The holistic operation of the FAM can be precisely defined as follows:

$$\begin{cases} Y_1 = CCAPM(X_H, X_L), \\ Y_2 = CCAPM(X_L, X_H), \\ Out = FUSE(Y_1, Y_2) \end{cases} \quad (6)$$

1) *Convolution & Cross Attention Parallel Module*: Building upon our prior observations, it becomes evident that both convolution and cross-attention mechanisms exhibit distinct advantages and limitations. The convolution operation manifests commendable strengths, including robust feature extraction capabilities, sparse connectivity, and notable computational and spatial efficiency. Nevertheless, it excels in

local information processing while potentially overlooking the broader global context, thereby omitting long-range dependencies. This inherent shortcoming can be effectively mitigated by harmonious collaboration with the cross-attention mechanism, which excels in capturing global dependencies but may not optimally emphasize local features. Furthermore, in contrast to the conventional self-attention mechanism, primarily adept at processing individual sequences from prior layers, we aspire to foster a more efficient synergy wherein two feature sequences, denoted as X_H and X_L , originating from the preceding layer, cohesively interact and mutually complement one another. In response to these considerations, we meticulously merge the cross-attention mechanism with convolution operations within our novel CCAPM. This judicious amalgamation facilitates the meaningful interaction of the extracted features, thereby enabling the comprehensive capture of intricate dependencies among them. Through the execution of this module, we acquire an enhanced capacity to aggregate the feature maps from the preceding layer, ultimately culminating in the refinement of embedded information.

The framework of our proposed Convolution & Cross-Attention Parallel Module (CCAPM) is shown in Figure 2. Specifically, two input features are processed by three **Feature Initialize (FI)** Blocks, each consisting of a 1×1 convolution and a ConvMixer block [32]. In this step, feature1 (X_H in the top branch, X_L in the bottom branch) is processed by one of these blocks, while feature2 is processed by two. Then, all those processed results are fed into two distinct pathways: convolution and cross-attention paths.

For the convolution path (eq. 7 and 8, take the top branch CCAPM as an illustrative example), three features are concatenated first and then fed into a fully connected layer.

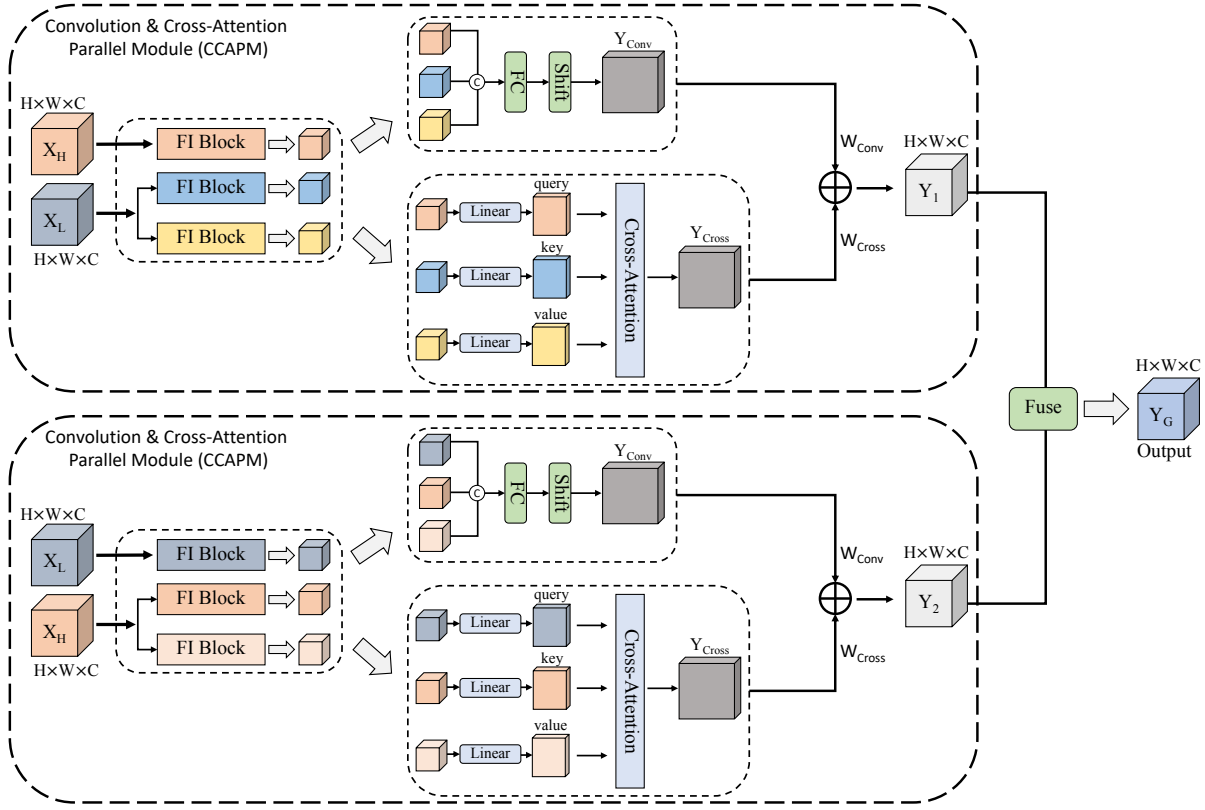


Fig. 2. The framework of our proposed Feature Aggregation Module (FAM).

Subsequent to this step, a shift operation is judiciously utilized to yield the ultimate output feature, denoted as Y_{conv} . Within the cross-attention path, three input features from the previous projected layer are meticulously fed into. Subsequent to linear embedding layers, these features are thoughtfully rendered as query (originating from feature1), key, and value, respectively. Consequently, these extracted features are introduced into the cross-attention mechanism, culminating in the derivation of the definitive outcome, dubbed as Y_{cross} . The final output is determined through the integration of these two paths, achieved by the addition of Y_{conv} and Y_{cross} , their respective contributions modulated by two learnable scalars (W_{Conv} and W_{Cross}), as delineated in eq. (9). Notably, Y_{out} from the top branch CCAPM represents Y_1 in eq. (6), while the Y_{out} from the bottom one represents Y_2 in eq. (6).

$$Y = \text{Concat}(FI_1(X_H), FI_2(X_L), FI_3(X_L)) \quad (7)$$

$$Y_{conv} = \text{Shift}(FC(Y)) \quad (8)$$

$$Y_{out} = W_{Conv} \times Y_{conv} + W_{Cross} \times Y_{cross} \quad (9)$$

2) *Fusion Block*: After two branches of CCAPM are performed, we utilize the simplified SKNet method [33] to merge the output features Y_1 and Y_2 adaptively. First, a global average pooling (GAP) is utilized to get the global information G_i as eq.(10). Next, G_1 and G_2 are stacked together, and then we use a channel-wise soft attention operation to generate feature importance vectors as eq.(11). Finally, under the guidance of the feature importance vector W_{g1} and W_{g2} ,

the channel-refined features Y_G can be obtained by merging the two features G_1 and G_2 as eq.(12).

$$G_i = \text{GAP}(Y_i) = \frac{1}{H \times W} \sum_{m=1}^H \sum_{n=1}^W Y_c(m, n), i = 1, 2 \quad (10)$$

$$\begin{cases} W_{g1} = \frac{e^{G_1}}{e^{G_1} + e^{G_2}} \\ W_{g2} = \frac{e^{G_2}}{e^{G_1} + e^{G_2}} \end{cases}, W_{g1} + W_{g2} = 1 \quad (11)$$

$$Y_G = W_{g1} \times G_1 + W_{g2} \times G_2 \quad (12)$$

C. Overall Architecture

The architecture of our proposed SCRNet is depicted in Figure 3. In keeping with the architectural principles initially presented in the UNet framework [1], we have conscientiously retained the encoder-decoder structure, a design choice that leverages the advantages of skip connections. This strategic adherence empowers us to capitalize on more feature-rich representations and, concomitantly, serves as a robust countermeasure against network degradation and the perils of overfitting.

Within our architectural framework, meticulous attention is directed towards the encoder block. It is here that we seamlessly incorporate the Spatial and Channel Refinement Module (SCRM) immediately following the convolutional block, which utilizes a 3×3 kernel with a stride of 1. This architectural design endows our model with the capacity to

selectively emphasize critical spatial and channel-related information while astutely attenuating extraneous data that may otherwise introduce interference within the network. Following the feature extraction phase, we utilize a max-pooling layer that serves the essential function of down-sampling the feature maps, skillfully preparing them for propagation to the ensuing network layer.

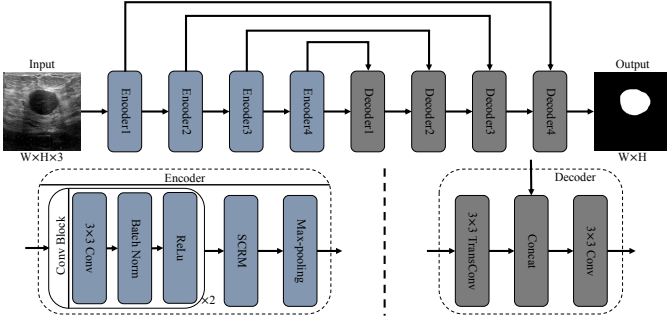


Fig. 3. The framework of our proposed Spatial-Channel Regulation Network (SCRNet). The Concat represents the channel-wise stack. We use 3×3 kernel with stride as 2 for Transpose Convolution (Transconv) in the decoder layers.

IV. EXPERIMENTS

A. Datasets and Evaluation Metrics

1) *Datasets*: The datasets utilized in our study are the Breast UltraSound Images (BUSI) dataset [34], BUSIS dataset [35], and TN3k dataset [36], [37]. The BUSI dataset, a widely recognized benchmark dataset, consists of 780 breast ultrasound images, focusing on benign and malignant cases (647 images) randomly split for training (453 images), validation (65 images), and testing (129 images). The BUSIS dataset includes 562 images obtained from women aged 26 to 78 years, the images were de-identified and sourced from different hospitals, with random splits for training (394 images), validation (56 images), and testing (112 images). Finally, the TN3k dataset contributes 3493 thyroid ultrasound images, following the official data split with 2879 images for training and validation and 614 images for testing.

2) *Evaluation Metrics*: We employ four commonly used metrics to perform a quantitative assessment of the performance of various segmentation models. These metrics include the Dice Similarity Coefficient (DSC), mean Intersection over Union (mIoU), Precision, and Recall.

B. Implementation Details

Training details. All of our experiments were conducted using PyTorch 1.7.0. We trained all models on a single NVIDIA RTX A6000 GPU with 48GB of memory. The Adam optimizer was employed with a learning rate annealing factor of 0.2, initializing at $1e-4$, and a weight decay of $5e-4$. As for the loss function, following the approach of [6], [7], we combined the dice loss and binary cross-entropy as defined in eq. (13).

$$Loss = Dice(pred, gt) + 0.5 \times BCE(pred, gt) \quad (13)$$

Data Preprocessing. Due to the limitation of the GPU memory, we use a batch size of 8 and train each model for 100 epochs. Besides, following the setting of [6] we resize all the images as $256 \times 256 \times 3$. Moreover, considering that insufficient data will induce overfitting, we apply data augmentation on the training set to alleviate this phenomenon. Specifically, we leverage random rotation, flip, elastic transform, and light transforms on the images with a probability of 0.5. Note that no operations were performed on the validation and test sets.

C. Results

We compare our methods with seven state-of-the-art models, such as UNet, ResUNet, AttUNet, TransUNet, UNeXt, CMUNet, and CMUNeXt. Results on BUSI and BUSIS datasets are shown in table I. Specifically, compared with the previous SOTA methods, for the BUSI dataset, our performance on mIoU and DSC have improved by 2.84% and 2.93%, respectively. For the BUSIS dataset, our performance on mIoU and DSC achieved improvement at 0.75% and 0.48%, respectively. Finally, as shown in table I, on the TN3K dataset, for mIoU and DSC, our proposed method brings out 1.22% and 1.12% improvement, respectively.

Some visualized results are shown in Figure 4, and it is evident that our proposed method excels in achieving more comprehensive nodule segmentation while minimizing disturbance compared to the competing methods. The images in Figure 4 illustrate that our model consistently produces impressive segmentation results across various scenarios, whether it's small nodules, large nodules, or particularly challenging nodules that closely resemble the background and are hard to differentiate. Furthermore, our model's segmentation results surpass those of other methods in terms of completeness, shape similarity to the ground truth (GT), and false positive regions. Notably, even when an image contains multiple nodules, our model adeptly segments them and effectively excludes interference from unrelated background regions. These visualized results underscore the superiority of our approach.

D. Ablation Study

Ablation study results are shown in table II. We can see from this table that, on the BUSI and BUSIS datasets, incorporating our SCRM but without the proposed FAM (replace the FAM by combining features via direct concatenation or summation operation, we report the better one) can bring **(0.89%, 0.72%)** and **(0.5%, 0.4%)** improvement on mIoU and DSC. Moreover, by combining our proposed FAM, those metrics will further increase by **(6.01%, 5.98%)** and **(0.64%, 0.33%)**. Simultaneously, on the TN3K dataset, results show that combining with SCRM (without the proposed FAM) can achieve **1.52%** and **0.99%** improvement on the mIoU and DSC metrics compared with the baseline model. However, compared with the methods leveraging our proposed FAM, those metrics are **2.47%** and **2.3%** lower. Therefore, the effectiveness of our proposed FAM and SCRM can be well demonstrated. Experimental results also have shown that the FAM is more indispensable.

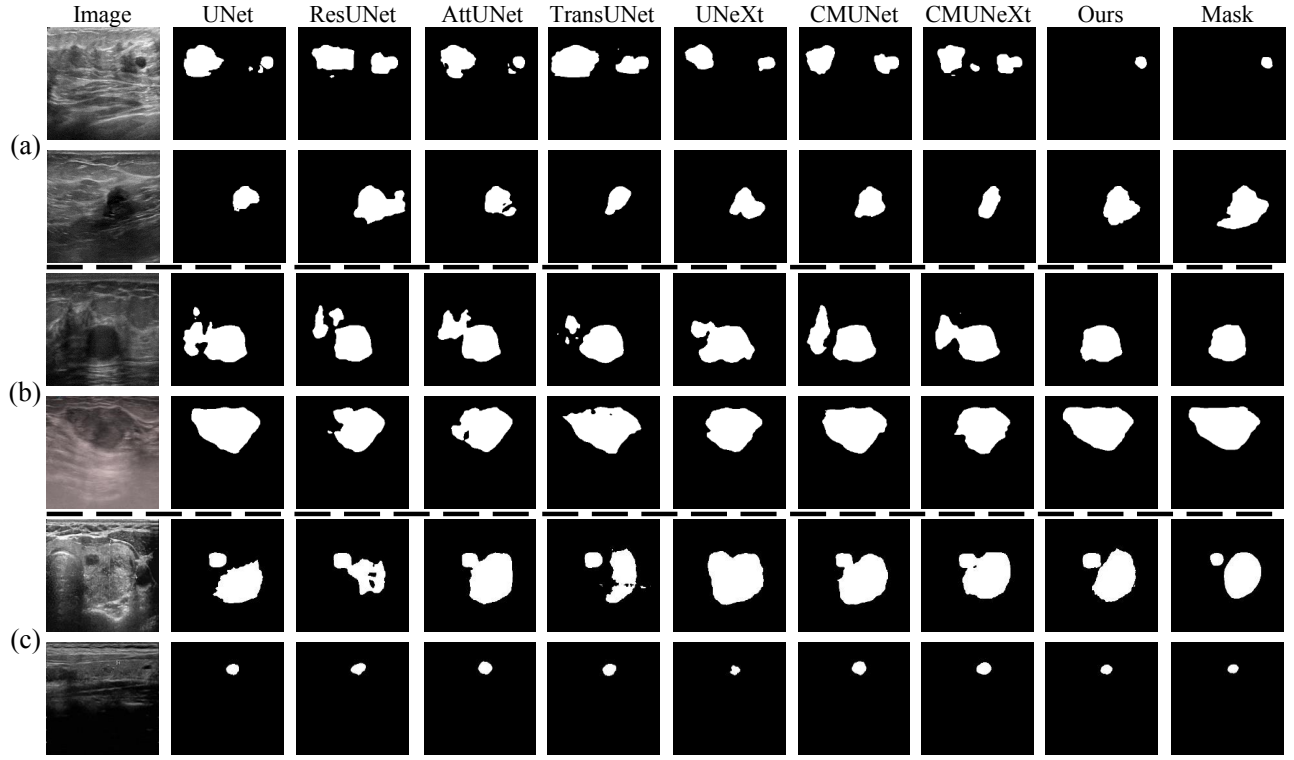


Fig. 4. Visualized results on BUSI, BUSIS, and TN3K datasets. From left to right are the input image, results of UNet, ResUNet, AttUNet, TransUNet, UNeXt, CMUNet, CMUNeXt, our proposed method, and the ground truth mask, respectively. (a) represents the segmentation results of benign and malignant nodules from the BUSI dataset; (b) represents segmentation results on the BUSIS dataset; and (c) represents results on the TN3K dataset.

TABLE I
COMPARISON RESULTS ON BUSI, BUSIS, AND TN3K DATASETS.

Methods	BUSI dataset (%)				BUSIS dataset (%)				TN3K dataset (%)			
	DSC	mIoU	Precision	Recall	DSC	mIoU	Precision	Recall	DSC	mIoU	Precision	Recall
UNet [1]	76.18	67.62	79.09	79.71	91.18	84.89	93.02	90.88	77.69	67.38	74.91	87.08
ResUNet [2]	77.27	68.45	79.20	80.36	91.26	85.09	93.18	91.15	76.76	66.67	73.93	86.18
AttUNet [5]	76.62	68.09	79.72	78.44	91.04	84.65	93.04	90.66	77.80	67.86	74.94	87.04
TransUNet [11]	71.94	61.88	78.57	73.57	89.97	82.69	90.09	91.53	71.65	60.03	69.37	83.13
UNeXt [38]	72.27	61.64	77.06	75.39	89.97	82.41	90.69	90.57	74.35	63.15	72.07	85.19
CMUNet [6]	79.95	71.68	84.13	81.45	91.43	85.28	92.86	91.58	79.86	70.15	78.35	85.19
CMUNeXt [7]	74.52	65.32	77.53	76.46	90.43	83.41	90.89	91.29	75.83	65.73	73.39	85.34
Ours	82.88	74.52	85.87	82.91	91.91	86.03	93.31	91.82	80.98	71.37	78.58	89.24

TABLE II
ABLATION STUDY RESULTS.

Methods (BUSI)	Metrics (%)			
	DSC	mIoU	Precision	Recall
UNet [1]	76.18	67.62	79.09	79.71
Ours w/o FAM	76.90	68.51	77.78	78.52
Our Model	82.88	74.52	85.87	82.91
Methods (BUSIS)	Metrics (%)			
	DSC	mIoU	Precision	Recall
UNet [1]	91.18	84.89	93.02	90.88
Ours w/o FAM	91.58	85.39	92.75	91.76
Our Model	91.91	86.03	93.31	91.82
Methods (TN3K)	Metrics (%)			
	DSC	mIoU	Precision	Recall
UNet [1]	77.69	67.38	74.91	87.08
Ours w/o FAM	78.68	68.90	75.74	87.48
Our Model	80.98	71.37	78.58	89.24

V. CONCLUSION

In this paper, we introduce a novel framework for medical image segmentation called SCRNet to enhance segmentation

accuracy and feature refinement. The cornerstone of our approach is the introduction of a novel Feature Aggregation Module (FAM) that effectively processes features extracted from the previous layer, facilitating enhanced feature interactivity. By strategically combining convolution and cross-attention mechanisms within the FAM, we can refine features more effectively, capturing both long-range dependencies and local context information. Furthermore, we introduce the FAM into the Spatial-Channel Regulation Module (SCRM), which replaces conventional concatenation or summation operations. The SCRM distinguishes between informative and non-informative features, allowing us to prioritize important information while mitigating interference from redundant features. To complete our framework, we integrate the SCRM into the encoder layers of the UNet architecture, resulting in SCRNet, which is tailored for medical ultrasound image segmentation.

REFERENCES

- [1] O. Ronneberger, P. Fischer, and T. Brox, "U-net: Convolutional networks for biomedical image segmentation," in *Medical Image Computing and Computer-Assisted Intervention—MICCAI 2015: 18th International Conference, Munich, Germany, October 5-9, 2015, Proceedings, Part III*. Springer, 2015, pp. 234–241.
- [2] Z. Zhang, Q. Liu, and Y. Wang, "Road extraction by deep residual u-net," *IEEE Geoscience and Remote Sensing Letters*, vol. 15, no. 5, pp. 749–753, 2018.
- [3] Z. Zhou, M. M. R. Siddiquee, N. Tajbakhsh, and J. Liang, "Unet++: Redesigning skip connections to exploit multiscale features in image segmentation," *IEEE transactions on medical imaging*, vol. 39, no. 6, pp. 1856–1867, 2019.
- [4] H. Huang, L. Lin, R. Tong, H. Hu, Q. Zhang, Y. Iwamoto, X. Han, Y.-W. Chen, and J. Wu, "Unet 3+: A full-scale connected unet for medical image segmentation," in *ICASSP 2020-2020 IEEE international conference on acoustics, speech and signal processing (ICASSP)*. IEEE, 2020, pp. 1055–1059.
- [5] O. Oktay, J. Schlemper, L. L. Folgoc, M. Lee, M. Heinrich, K. Misawa, K. Mori, S. McDonagh, N. Y. Hammerla, B. Kainz *et al.*, "Attention u-net: Learning where to look for the pancreas," *arXiv preprint arXiv:1804.03999*, 2018.
- [6] F. Tang, L. Wang, C. Ning, M. Xian, and J. Ding, "Cmu-net: a strong convmixer-based medical ultrasound image segmentation network," in *2023 IEEE 20th International Symposium on Biomedical Imaging (ISBI)*. IEEE, 2023, pp. 1–5.
- [7] F. Tang, J. Ding, Q. Quan, L. Wang, C. Ning, and S. K. Zhou, "Cmunext: An efficient medical image segmentation network based on large kernel and skip fusion," in *2024 IEEE International Symposium on Biomedical Imaging (ISBI)*. IEEE, 2024, pp. 1–5.
- [8] J. Li, Y. Wen, and L. He, "Sconv: Spatial and channel reconstruction convolution for feature redundancy," in *Proceedings of the IEEE/CVF Conference on Computer Vision and Pattern Recognition*, 2023, pp. 6153–6162.
- [9] A. Vaswani, N. Shazeer, N. Parmar, J. Uszkoreit, L. Jones, A. N. Gomez, L. Kaiser, and I. Polosukhin, "Attention is all you need," *Advances in neural information processing systems*, vol. 30, 2017.
- [10] A. Dosovitskiy, L. Beyer, A. Kolesnikov, D. Weissenborn, X. Zhai, T. Unterthiner, M. Dehghani, M. Minderer, G. Heigold, S. Gelly *et al.*, "An image is worth 16x16 words: Transformers for image recognition at scale," *arXiv preprint arXiv:2010.11929*, 2020.
- [11] J. Chen, Y. Lu, Q. Yu, X. Luo, E. Adeli, Y. Wang, L. Lu, A. L. Yuille, and Y. Zhou, "Transunet: Transformers make strong encoders for medical image segmentation," *arXiv preprint arXiv:2102.04306*, 2021.
- [12] O. Petit, N. Thome, C. Rambour, L. Themyr, T. Collins, and L. Soler, "U-net transformer: Self and cross attention for medical image segmentation," in *Machine Learning in Medical Imaging: 12th International Workshop, MLMI 2021, Held in Conjunction with MICCAI 2021, Strasbourg, France, September 27, 2021, Proceedings 12*. Springer, 2021, pp. 267–276.
- [13] H. Noh, S. Hong, and B. Han, "Learning deconvolution network for semantic segmentation," in *Proceedings of the IEEE international conference on computer vision*, 2015, pp. 1520–1528.
- [14] V. Badrinarayanan, A. Kendall, and R. Cipolla, "Segnet: A deep convolutional encoder-decoder architecture for image segmentation," *IEEE transactions on pattern analysis and machine intelligence*, vol. 39, no. 12, pp. 2481–2495, 2017.
- [15] H. Zhao, J. Shi, X. Qi, X. Wang, and J. Jia, "Pyramid scene parsing network," in *Proceedings of the IEEE conference on computer vision and pattern recognition*, 2017, pp. 2881–2890.
- [16] C. Szegedy, W. Liu, Y. Jia, P. Sermanet, S. Reed, D. Anguelov, D. Erhan, V. Vanhoucke, and A. Rabinovich, "Going deeper with convolutions," in *Proceedings of the IEEE conference on computer vision and pattern recognition*, 2015, pp. 1–9.
- [17] G. Lin, A. Milan, C. Shen, and I. Reid, "Refinenet: Multi-path refinement networks for high-resolution semantic segmentation," in *Proceedings of the IEEE conference on computer vision and pattern recognition*, 2017, pp. 1925–1934.
- [18] C. Yu, J. Wang, C. Peng, C. Gao, G. Yu, and N. Sang, "Learning a discriminative feature network for semantic segmentation," in *Proceedings of the IEEE conference on computer vision and pattern recognition*, 2018, pp. 1857–1866.
- [19] H. Zhao, Y. Zhang, S. Liu, J. Shi, C. C. Loy, D. Lin, and J. Jia, "Psanet: Point-wise spatial attention network for scene parsing," in *Proceedings of the European conference on computer vision (ECCV)*, 2018, pp. 267–283.
- [20] S. Zheng, J. Lu, H. Zhao, X. Zhu, Z. Luo, Y. Wang, Y. Fu, J. Feng, T. Xiang, P. H. Torr *et al.*, "Rethinking semantic segmentation from a sequence-to-sequence perspective with transformers," in *Proceedings of the IEEE/CVF conference on computer vision and pattern recognition*, 2021, pp. 6881–6890.
- [21] F. Zhu, Y. Zhu, L. Zhang, C. Wu, Y. Fu, and M. Li, "A unified efficient pyramid transformer for semantic segmentation," in *Proceedings of the IEEE/CVF International Conference on Computer Vision*, 2021, pp. 2667–2677.
- [22] W. Wang, E. Xie, X. Li, D.-P. Fan, K. Song, D. Liang, T. Lu, P. Luo, and L. Shao, "Pyramid vision transformer: A versatile backbone for dense prediction without convolutions," in *Proceedings of the IEEE/CVF international conference on computer vision*, 2021, pp. 568–578.
- [23] E. Xie, W. Wang, Z. Yu, A. Anandkumar, J. M. Alvarez, and P. Luo, "Segformer: Simple and efficient design for semantic segmentation with transformers," *Advances in Neural Information Processing Systems*, vol. 34, pp. 12077–12090, 2021.
- [24] R. Strudel, R. Garcia, I. Laptev, and C. Schmid, "Segmenter: Transformer for semantic segmentation," in *Proceedings of the IEEE/CVF international conference on computer vision*, 2021, pp. 7262–7272.
- [25] Y. Zhou, H. Chang, X. Lu, and Y. Lu, "Denseunet: Improved image classification method using standard convolution and dense transposed convolution," *Knowledge-Based Systems*, vol. 254, p. 109658, 2022.
- [26] D. Jha, P. H. Smedsrud, D. Johansen, T. de Lange, H. D. Johansen, P. Halvorsen, and M. A. Riegler, "A comprehensive study on colorectal polyp segmentation with resunet++, conditional random field and test-time augmentation," *IEEE journal of biomedical and health informatics*, vol. 25, no. 6, pp. 2029–2040, 2021.
- [27] Z. Li, D. Li, C. Xu, W. Wang, Q. Hong, Q. Li, and J. Tian, "Tfcns: A cnn-transformer hybrid network for medical image segmentation," in *International Conference on Artificial Neural Networks*. Springer, 2022, pp. 781–792.
- [28] Y. Chenyu, R. Zhao, F. Liu, S. Chinchali, U. Topcu, L. Staib, and J. S. Duncan, "Class-aware generative adversarial transformers for medical image segmentation," *arXiv preprint arXiv:2201.10737*, 2022.
- [29] H. Cao, Y. Wang, J. Chen, D. Jiang, X. Zhang, Q. Tian, and M. Wang, "Swin-unet: Unet-like pure transformer for medical image segmentation," in *European conference on computer vision*. Springer, 2022, pp. 205–218.
- [30] Z. Liu, Y. Lin, Y. Cao, H. Hu, Y. Wei, Z. Zhang, S. Lin, and B. Guo, "Swin transformer: Hierarchical vision transformer using shifted windows," in *Proceedings of the IEEE/CVF international conference on computer vision*, 2021, pp. 10012–10022.
- [31] Y. Wu and K. He, "Group normalization," in *Proceedings of the European conference on computer vision (ECCV)*, 2018, pp. 3–19.
- [32] A. Trockman and J. Z. Kolter, "Patches are all you need?" *arXiv preprint arXiv:2201.09792*, 2022.
- [33] X. Li, W. Wang, X. Hu, and J. Yang, "Selective kernel networks," in *Proceedings of the IEEE/CVF conference on computer vision and pattern recognition*, 2019, pp. 510–519.
- [34] W. Al-Dhabyani, M. Gomaa, H. Khaled, and A. Fahmy, "Dataset of breast ultrasound images," *Data in brief*, vol. 28, p. 104863, 2020.
- [35] Y. Zhang, M. Xian, H.-D. Cheng, B. Shareef, J. Ding, F. Xu, K. Huang, B. Zhang, C. Ning, and Y. Wang, "Busis: a benchmark for breast ultrasound image segmentation," in *Healthcare*, vol. 10, no. 4. MDPI, 2022, p. 729.
- [36] H. Gong, J. Chen, G. Chen, H. Li, F. Chen, and G. Li, "Thyroid region prior guided attention for ultrasound segmentation of thyroid nodules," *Computers in Biology and Medicine*, vol. 106389, pp. 1–12, 2022.
- [37] H. Gong, G. Chen, R. Wang, X. Xie, M. Mao, Y. Yu, F. Chen, and G. Li, "Multi-task learning for thyroid nodule segmentation with thyroid region prior," in *2021 IEEE 18th International Symposium on Biomedical Imaging (ISBI)*, 2021, pp. 257–261.
- [38] J. M. J. Valanarasu and V. M. Patel, "Unext: Mlp-based rapid medical image segmentation network," in *International Conference on Medical Image Computing and Computer-Assisted Intervention*. Springer, 2022, pp. 23–33.